PCCP

# Osteocalcin Facilitates Calcium Phosphate Ion Complex Growth as Revealed by Free Energy Calculation


| | |
|---|---|
| Journal: | *Physical Chemistry Chemical Physics* |
| Manuscript ID | CP-ART-02-2018-001105.R1 |
| Article Type: | Paper |
| Date Submitted by the Author: | 08-Apr-2018 |



| | |
|---|---|
| Complete List of Authors: | Zhao, Weilong; University of Akron, Polymer Science<br>Wang, Ziqiu; University of Akron, Polymer Science<br>Xu, Zhijun; Nanjing Tech University,<br>Sahai, Nita; University of Akron, Polymer Science |

*Physical Chemistry Chemical Physics – Revision 1*

# Osteocalcin Facilitates Calcium Phosphate Ion Complex Growth as Revealed by Free Energy Calculation

*Weilong Zhao[1], Ziqiu Wang[1], Zhijun Xu[2], and Nita Sahai[1,3*]*

[1]Department of Polymer Science, University of Akron, 170 University Ave, Akron, Ohio 44325-3909, United States.

[2]College of Chemical Engineering, State Key Laboratory of Materials-Oriented Chemical Engineering, Nanjing Tech University, Nanjing 210009, China.

[3]Department of Geology and Integrated Bioscience Program, University of Akron, Akron, Ohio 44325-3909, United States

*Corresponding author: Nita Sahai, sahai@uakron.edu. Telephone: 330-972-5795

**Abstract**

The nanoscopic structural and thermodynamic basis of biomolecule-regulated assembly and crystallization of inorganic solids have tremendous impact on the rational design of novel functional nanomaterials, but are concealed by many difficulties in molecular-level characterization. Here we demonstrate that the free energy calculation approach, enabled by combining advanced molecular simulation techniques, can unravel the structural and energetic mechanisms of protein-mediated inorganic solid nucleation. It is observed that osteocalcin (OCN), an important non-collagenous protein involved in regulating bone formation, promotes the growth of nanosized calcium phosphate (CaP) ion clusters from supersaturated solution. Free energy calculation by umbrella sampling indicates that this effect by OCN is prominent at the scale of 1 to 3 nm ion-association complexes (IACs). The binding interactions between gamma-carboxyl glutamate and C-terminal and, interestingly, the arginine side chains of OCN with IACs stabilize under-coordinated IACs, thus promoting their growth. The promotor effect of OCN on the enlargement and further aggregation of IACs into cluster assemblies of 10s nm, are confirmed by conventional molecular dynamics simulation and dynamic light scattering experiment. To the best of our knowledge, this is the first time that the free energy landscape of the early stages of CaP nucleation is shown. The free energy change as a function of IAC size shares the feature of decreasing monotonically as shown previously for the calcium carbonate system. Therefore, the nucleation of both these two major biominerals apparently involves an initial phase of liquid-like ionic aggregates. The structural and thermodynamic information regarding OCN-CaP interactions amplify the current understanding of biomineralization mechanisms at the nanoscale, with general relevance to biomolecule-tuned fabrication of inorganic materials.

## 1. Introduction

Biomolecule-directed assemblies of materials at nanoscale lead to complex and delicate microscopic structures with a wide spectrum of functions, including optical, electronical, and mechanical.[1-4] For example, one unique role of proteins constituting the macromolecular matrix in living organisms is manipulating the formation of mineralized tissues such as calcium phosphate (CaP) mineral in the endoskeleton of vertebrates, and calcium carbonate minerals in exoskeletons of invertebrates.[5-7] The nucleation and growth of mineral phases in biological tissues are regulated by complex signaling pathways that involve both protein-protein and protein-mineral association.[8,9] While the detailed mechanisms of how proteins interact with biominerals remain controversial, it is believed that proteins either present as organized substrates for the heterogeneous nucleation of minerals,[10] and/or sequester the inorganic ions or ion-complexes that are available in solution for homogeneous crystallization.[11,12] At the atomic level, protein-mineral interactions are governed by direct or water-mediated binding between protein amino acid side chains and inorganic ions.[13,14] In general, although protein-controlled inorganic particle nucleation and growth are considered as the theoretical models to facilitate the rational design of composite nanomaterials, the relevant structural and thermodynamic information at the nanoscale remain poorly understood.[15]

In the present study, we focus on protein-controlled inorganic nucleation in the specific case of bone biomineralization. Non-stoichiometric hydroxyapatite (HAP, idealized stoichiometry $Ca_{10}(PO_4)_6(OH)_2$) comprises the inorganic component of bone, and the crystals have a plate-like morphology.[16,17] The nucleation and growth of HAP plate-like crystals in the extracellular matrix (ECM) are thought to be controlled cooperatively by insoluble

collagen fibrils, soluble non-collagenous proteins (NCPs), and potentially, small molecules.[6,12,13,18,19] Body fluid contains calcium ($Ca^{2+}$) and phosphate ($H_2PO_4^-/HPO_4^{2-}$) ions that are concentrated enough to be supersaturated with respect to HAP, but the spontaneous precipitation of HAP is inhibited except in bone and teeth. This phenomenon indicates that the deposition of CaP inside the self-assembled collagen matrix is regulated by the presence of collagen and NCPs. Osteocalcin (OCN), also known as bone γ-carboxyglutamic acid (Gla)-containing protein, is a NCP secreted solely by osteoblasts and thought to play an essential role in bone metabolism and mineralization.[20,21] Often used as a biomarker for detecting bone mineral formation, the function of OCN in controlling HAP nucleation and growth remain unclear. While it has been shown that the Gla domain of OCN binds to $Ca^{2+}$ in its native state[22], little experimental evidence exists to unequivocally support that OCN is effective in regulating mineralization locally in the ECM. Various *in vivo* experiments on mouse knockout models have presented diverse results. Deficiency of OCN expression enhanced bone mineral formation,[23] whereas elevated gene expression did not result in suppression of mineralization.[24] Recently, it has been demonstrated by immunolocalization and gene expression assay that the location of OCN in mineralizing turkey tendon is associated preferentially with the mineralized segments.[25] Compared to most other NCPs involved in bone mineralization, a distinctive feature of OCN is that it possesses a native 3-D crystal structure, which was obtained by XRD for the porcine homological sequence (Figure S1).[22] Therefore, OCN serves as a challenging yet promising example to understand the molecular mechanisms of protein-controlled mineralization by computational approaches. In contrast to several key computational advances reported recently on the calcium carbonate

system, a theoretical consideration on the free energy landscape and molecular mechanism of CaP nucleation has yet to be established.

The *in vitro* nucleation and growth of HAP in the absence of any additives have been hypothesized to follow non-classical nucleation theory, as suggested by previous evidence from various electron microscope techniques.[26-29] In particular, ion-associated complexes (IACs) of 1 to 2 nm size emerge in solution phase, followed by their aggregation into amorphous calcium phosphate (ACP) particles of ~ 100 nm size.[26] The ACP particles can enlarge by the attachment of IACs, then dehydrate and transform to the crystalline phases of CaP.[29-31] The exact mechanisms of the phase transitions between IACs, ACP, and HAP are hotly debated. One hypothesis proposed that IACs are distinguishable species in supersaturated solution, and may be stabilized by a liquid-liquid phase separation, a process that is known in protein crystallization.[32,33] Although the concept of oligomeric ionic species is well established in the literature, for instance the Keggin anion and other polyoxometalates,[34,35] IACs are different in that they do not form well-defined stereo-structures, and are generally aqueous multi-nuclear complexes of ionic salts.

The potential role of proteins as organic substrates in the initial stages of forming IACs also remains obscure. Despite recent efforts on model systems of heterogeneous nucleation of CaP,[26,27,36] no study exists for an actual NCP. Considering the critical function of proteins in directing the crystallization of inorganic phases, the current understanding of the interaction between NCPs with liquid phase species, such as IACs, is unsatisfying.

In our previous studies, the molecular-level mechanisms of CaP nucleation in the presence of organic substrates have been addressed by a combination of molecular dynamics (MD) simulation and experimental approaches.[37,38] We have demonstrated by MD simulation

that assembled collagen fibrils as well as another NCP, bone sialoprotein, both promote the formation of nanosized CaP ion complexes.[37,38] The molecular interactions of this effect are dominated by the electrostatic attraction between the charged side chains of proteins with $Ca^{2+}$ and $HPO_4^{2-}$ ions, leading to the stabilization of ion complexes in the vicinity of the proteins. These results revealed that the charged side chain moieties on proteins provide binding sites for inorganic species and can potentially promote their nucleation from either individual ions or IACs. However, the free energy landscape for IAC formation was not examined as the emphasis in the prior studies was on structural details of the mechanisms. In the present study, we attempted (i) to calculate free energy of the formation pathway of nanoscale CaP clusters in the reference system without OCN, and (ii) to elucidate the effect of OCN in the early stages of CaP formation. The free energy landscape of reactions provides the most important information for revealing inorganic nucleation and growth mechanisms.[39]

A major obstacle preventing the application of conventional MD towards acceptably accurate estimation of free energy is the difficulty in sampling CaP (or other ionic salt) nucleus formation in an accessible modeling timeframe, because of high energy barriers associated with electrostatic forces and explicit solvation. Enhanced-sampling techniques are much needed to overcome efficiently the energy barriers.[40,41] As exemplified by previous simulations on various inorganic systems,[42-45] advanced MD sampling techniques allow detailed exploration of the structure and free energy landscape along the nucleation pathway. We employed metadynamics (MetaD),[46] a method devised to enhance conformational sampling by aggressively perturb the free energy surface of complex phase transformations.[47,48] In the current study, MetaD facilitated the exploration of CaP nucleation pathway by sampling the ion complexes over a range of sizes and permitted the construction

of free energy landscape of ion complex formation. Following MetaD, Umbrella Sampling (US) simulation was used to calculate the free energy of CaP ion complex nucleation by defining appropriate collective variables (CVs). Examining the initial stages of nucleation requires accounting for transient liquid phase species. These transient liquid phase species were characterized by a CV designating the maximum size of a population of ion complexes of different sizes. By combining MetaD and US, our calculations concern not only the free energy of nanosized CaP ion complex formation from inorganic aqueous solution, but also the effect of OCN as an organic substrate in this process. We also used conventional MD simulations to model the aggregation of IACS to larger cluster assemblies and dynamic light scattering experiments to explore aggregation of the cluster assemblies to amorphous calcium phosphate (ACP) particles. The molecular structural and thermodynamic data from our studies reveal that, binding of ions and ion pairs to charged side chains of OCN reduces the free energy of phase transformation from dissolved ions to nanosized ion complexes, such that OCN has the effect of promoting initial CaP nucleation. Subsequently, OCN kinetically facilitates the growth of the IACs by attachment of smaller ones to form ACP nanoparticles.

## 2. Results and Discussion

*Relative Free Energies of Ion Complex Formation*

A major limitation in the application of MD simulation in the biomineralization literature has been the difficulty to sample accurately CaP nucleus formation in accessible modeling timeframes. The application of MetaD in our study using the two CVs facilitates energy barrier-crossing. For both the reference system without OCN (Ion-Ref) and the system with OCN (Ion-OCN), ion complexes are observed to have comparable size distribution, which then allows for the extraction of configurations for free energy calculation within a similar CV range. In the absence of efficient energy barrier-crossing, the conventional MD results in the formation of ion complexes that are smaller and do not preferentially attach to OCN side chains (Figure S2). The effect of MetaD on accelerating the sampling of complex configurations is quantified by calculating the Maximum Complex Size (MCS) and the average complex size as a function of time (Figure S2). The MetaD simulations also hasten the configurational sampling of the coordination structure of complexes under explicit solvation. As noted previously, the inclusion of global explicit solvation and salt concentration in simulation is indispensable to the determination of transient ionic species at corresponding experimental conditions.[45,49] The results of our MetaD simulations suggest that the speed of phase space exploration was largely enhanced, compared with classical MD (Figure S2). By accelerating the spontaneous association of ions, MetaD leads to important intermediates in cluster formation.

The intermediate states sampled from MetaD are used to calculate PMF profiles by US (Figure 1). The comparable height of CV probability histograms (Figure 1, inset) confirms that MCS of each window has been adequately sampled. Starting from MCS = 3,

the free energy of both systems monotonically decreases until the complex size reaches MCS = 13. Notably, no significant free energy basin is observed for either PMF curves, indicating that the ion complex growth is a thermodynamically downhill process and does not incur any energy barrier. Secondly, taking into account the statistical analysis, it is evident that the Ion-Ref system indeed has higher free energy compared to the Ion-OCN system. Because the reaction coordinate for free energy is defined as the ion complex size, this difference indicates that the growing complexes in the Ion-OCN system have advantage over the reference system to attach additional free ions or ion pairs and form larger complexes.

Our calculations provided relative energy landscape with respect to our particularly defined CV, indicating thermodynamic stability of certain structural geometries. This information is not suitable for directly being used as a measure of absolute free energy value, which can only be obtained by density functional theory. However, the relative free energy change we obtained here reveals a thermodynamic basis for OCN-promoted initial growth of ion complexes at the initial nucleation stage. To the best of our knowledge, this is the first time that such information has been shown for CaP nucleation.

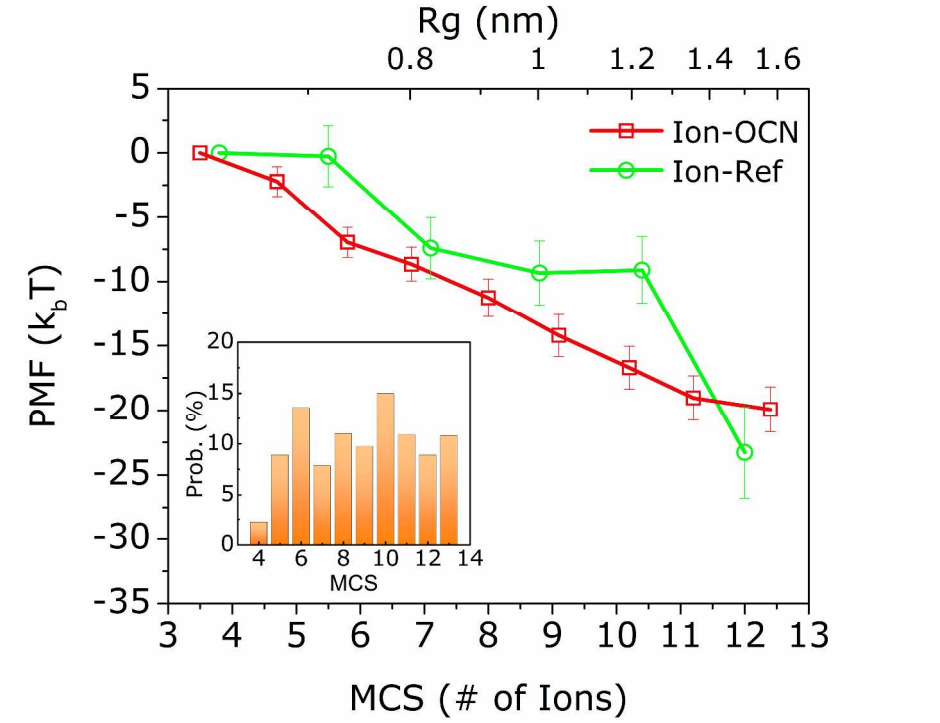


Figure 1. Free energy profiles of CaP complex growth from 3 to 13 ions by US simulation. The error bars shown are estimated by bootstrap analysis of MBAR.[50] The upper x-axis indicates average radius of gyration (Rg) of the CaP complexes sampled by the corresponding US window. Inset: the histogram of umbrella restraint-biased MCS distributions for the Ion-OCN system. As a result of restraint potentials, each bin has comparable volume of sampled configurational states.

*Structural Analysis of Ion Complex*

We investigated the origin of the free energy difference between various complexes in the absence and presence of OCN by further examining their structures at the molecular-level (Figure 2). Despite the fluctuation of MCS within each window, the most probable molecular configuration can still be determined by MBAR reweighting. Two end states (MCS = 4 and 13) and one intermediate state (MCS = 9) are chosen on the PMF curves and their microscopic configurations are extracted, respectively, for the Ion-Ref and the Ion-OCN systems. At MCS = 4 (Figure 2a), the largest complex in the Ion-OCN system is found in solution rather than bound to the protein. This complex has similar structure in both systems with two $Ca^{2+}$ and two $HPO_4^{2-}$ ions. Smaller "complexes" in both systems exist either as individual ions or as ion pairs.

Significant structural differences between Ion-Ref and Ion-OCN systems are observed when complexes grow to MCS = 9 (Figure 2b). In the reference system, the complex has $6Ca^{2+}$-$3HPO_4^{2-}$ composition and its net charge has to be offset by bound water molecules and $Cl^-$ ions. For the Ion-OCN system, the largest complex is also comprised of six $Ca^{2+}$ and three $HPO_4^{2-}$ ions and it binds to the Gla side chains of OCN. Thus, OCN mediates CaP nucleation through these side chains, which may act as the "anion" to balance the net positive charge of the complex, instead of water and $Cl^-$ ions. This scenario may be responsible for the lower free energy of complex formation than the reference system.[51] We note that, while it has been hypothesized that the side chain position and orientation of OCN may provide a "lattice match" to the $Ca^{2+}$ ions on the surface of HAP crystal,[52] the molecular configurations from our simulation do not provide such evidence. Instead, it is observed that the relative distances between the two Gla side chains are constantly fluctuating, leading to a

changing of bound $Ca^{2+}$-$Ca^{2+}$ distance as well. Thus, it is more likely that the Gla segment offers a negatively charged molecular motif to bind $Ca^{2+}$ ions and reduces the degree of under-coordination of the CaP complexes.

Interestingly, instead of binding to the Gla segment, the largest complex extracted from the US window of MCS = 13 is identified to bind to the C-terminal of OCN, which has two charged residues of arginine (Arg) (Figure 2c, middle). Both C-terminal and Arg residue side chain participate in binding with the ion complex. The involvement of the Arg residue biding $HPO_4^{2-}$ ions is interesting because it has been previously assumed in the literature that OCN only interacts with $Ca^{2+}$ ions through the Gla residues. Although a configuration of ion complex binding to the Gla segment is also observed in the US simulation (Figure 2c, right), this configuration has less sampled probability compared to that at the C-terminal. Therefore, we infer that while the Gla segment still contributes to the stability and facilitates the growth of the ion complexes, electrostatic attraction force generated by OCN at other charged side chains is potentially more important in sequestering ion complexes of these large sizes. Comparing the PMFs at the state of MCS = 13 indicates that both Ion-Ref and Ion-OCN systems have very similar free energies (Figure 1). This result suggests that the presence of OCN does not exert a thermodynamic advantage for complexes of this size. Thus, at these large sizes of ion complex, the detail of which site on OCN is involved in binding seems less relevant than at the intermediate sizes. This is a novel insight revealed by the present study.

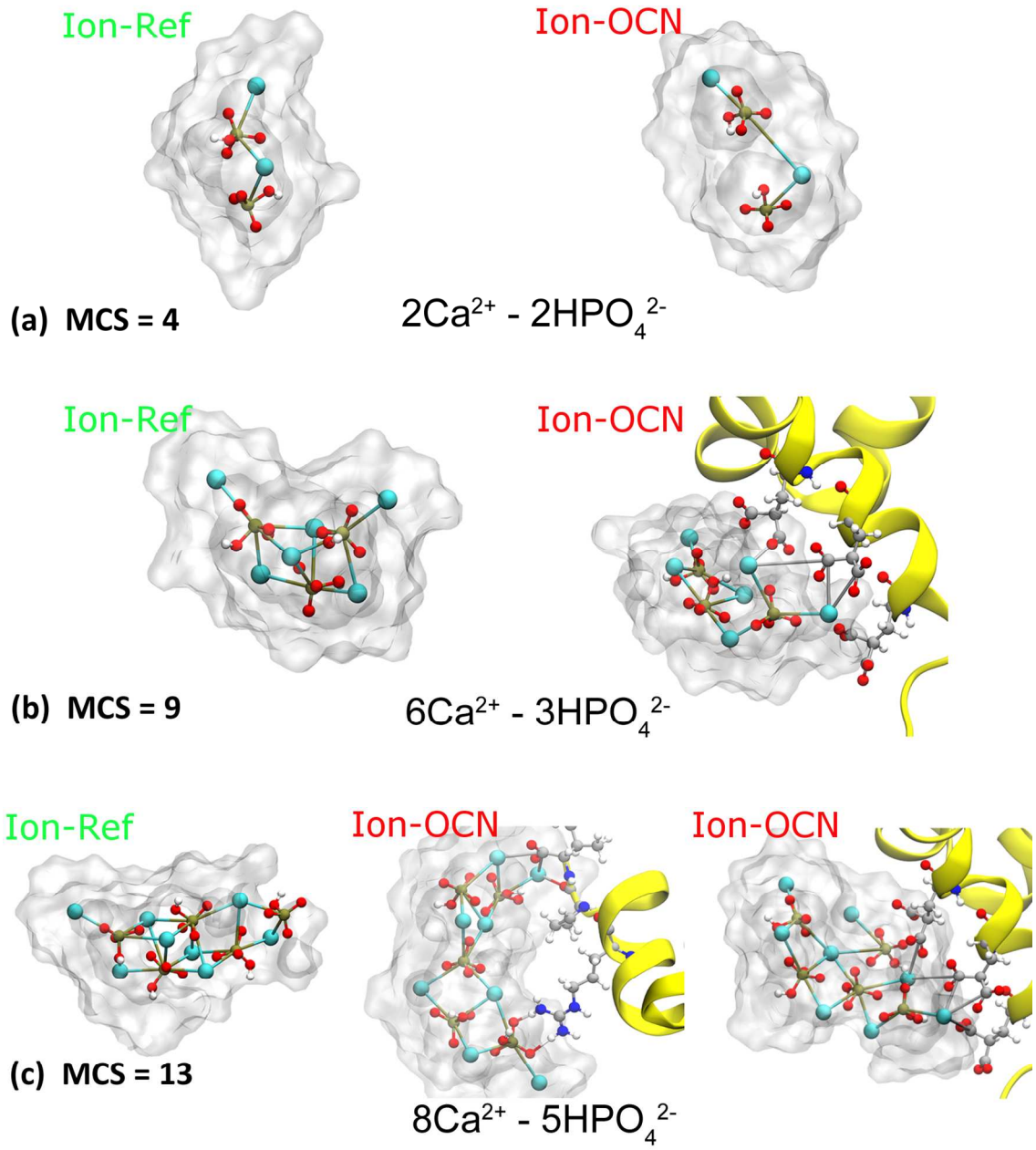


Figure 2. The representative configurations collected from different sampling windows of US simulations for (a) MCS = 4; (b) MCS = 9; and (c) MCS = 13. The simulation system is specified as labeled. The backbone of OCN is represented by yellow ribbon in (a). Color designation for atoms: cyan: calcium; red: oxygen; tan: phosphorus; white: hydrogen; grey: carbon; blue: nitrogen. The solvation shells of ion cluster within the cutoff of 3.5 Å are shown as transparent molecular surface. Bulk water molecules and $Na^+$ and $Cl^-$ ions are not shown for clarity.

The binding of OCN side chains with the ion complexes not only affects their free energy of growth, but also impacts their coordination chemistry. As shown in Figure 3, there is an obvious difference between systems without and with OCN, with respect to the distribution of $HPO_4^{2-}$ to $Ca^{2+}$ coordination number (CN(P-Ca)). Only a small fraction of ion complexes in the reference system have an average CN(P-Ca) = ~1, while a substantial proportion have included an extra $HPO_4^{2-}$ to elevate the average CN(P-Ca) to ~1.3 (Figure 3a, left). On the contrary, a number of ion complex configurations of the Ion-OCN system have CN(P-Ca) slightly larger than 1 (Figure 3b, left), as a result of $Ca^{2+}$ coordinated either by one or two $HPO_4^{2-}$ ions. The under-coordination of $Ca^{2+}$ ions in the complexes is compensated by binding with Gla side chains. The structure of the ion complex in the reference system includes tri-coordinated $Ca^{2+}$ (Figure 3a, right). For the Ion-OCN system, such tri-coordinated $Ca^{2+}$ ions are only observed in the large complexes (MCS = 13 or 14) bound to the C-terminal of OCN (Figure 3b, right). Evidently, the presence of OCN changes of the coordination symmetry of nanosized CaP complexes by providing ionic coordination from the charged side chains. With respect to the morphology of the complexes, elongated, ribbon-like polymeric structures are observed in both the Ion-Ref and Ion-OCN systems, suggesting a high level of hydration and large solvent-accessible surface areas of the ion complexes.

The IAC species proposed by Habraken et al. for the inorganic Ca-P system have a predominant composition of calcium triphosphate ($Ca(HPO_4)_3^{4-}$),[26] which later binds an extra $Ca^{2+}$ to form ($Ca_2(HPO_4)_3^{2-}$), the constituting element of large ACP particles. The tendency of $Ca^{2+}$ to be coordinated by three $HPO_4^{2-}$ ions is also observed in our simulation for both systems, especially in the reference system (Figure 3). It can be seen that the $Ca^{2+}$ coordinated in the interior region of the ion complexes are generally surrounded by three

$HPO_4^{2-}$ ions, especially for the reference system (Figure 3, pink Ca atoms). Furthermore, the 2-D probability distribution of states shows contour distribution of CN(P-Ca) around 1.5 in the reference system (Figure 3a), which concurs with a composition of $Ca_2(HPO_4)_3^{2-}$ identified experimentally as the characteristic stoichiometry of complexes in the aggregation of IACs to ACP.[26]

In the Ion-OCN system, although complexes of $Ca_2(HPO_4)_3^{4-}$ composition are not detected in IACs that are smaller than 10 ions, the elongate-shaped complexes bound to the side chains of OCN are available for further compositional change by incorporating additional $Ca^{2+}$ ions. This step may potentially lead an increase in CN(P-Ca), as shown by the dense contour distribution around 1.5 at larger complex sizes (Figure 3a, bottom). In addition, in the presence of $H_2PO_4^{2-}$ ions, which are not included in our simulations, the stoichiometric ratio of phosphate to $Ca^{2+}$ ions may further increase, leading to the formation of calcium triphosphate that is consistent with the previous experimental results.[26] In summary, the ion complexes discovered here have high similarity in stoichiometry with previous experimentally-defined IAC species.

The complexes observed from our simulations of both systems have elongated rather than spherical shape, with aspect ratios ranging from 2 to 3 (Figure 3). The contour diagram of MCS versus coordination number shows substantial peaks at CN(P-Ca) < 2, which corroborates the previous experimental observation, that most CaP complexes have anisotropic shapes.[26] The interactions between water and CaP atoms are essential to form this geometry. More substantial conformational sampling using CVs particularly related to water molecules will be required to further elucidate the detailed information.

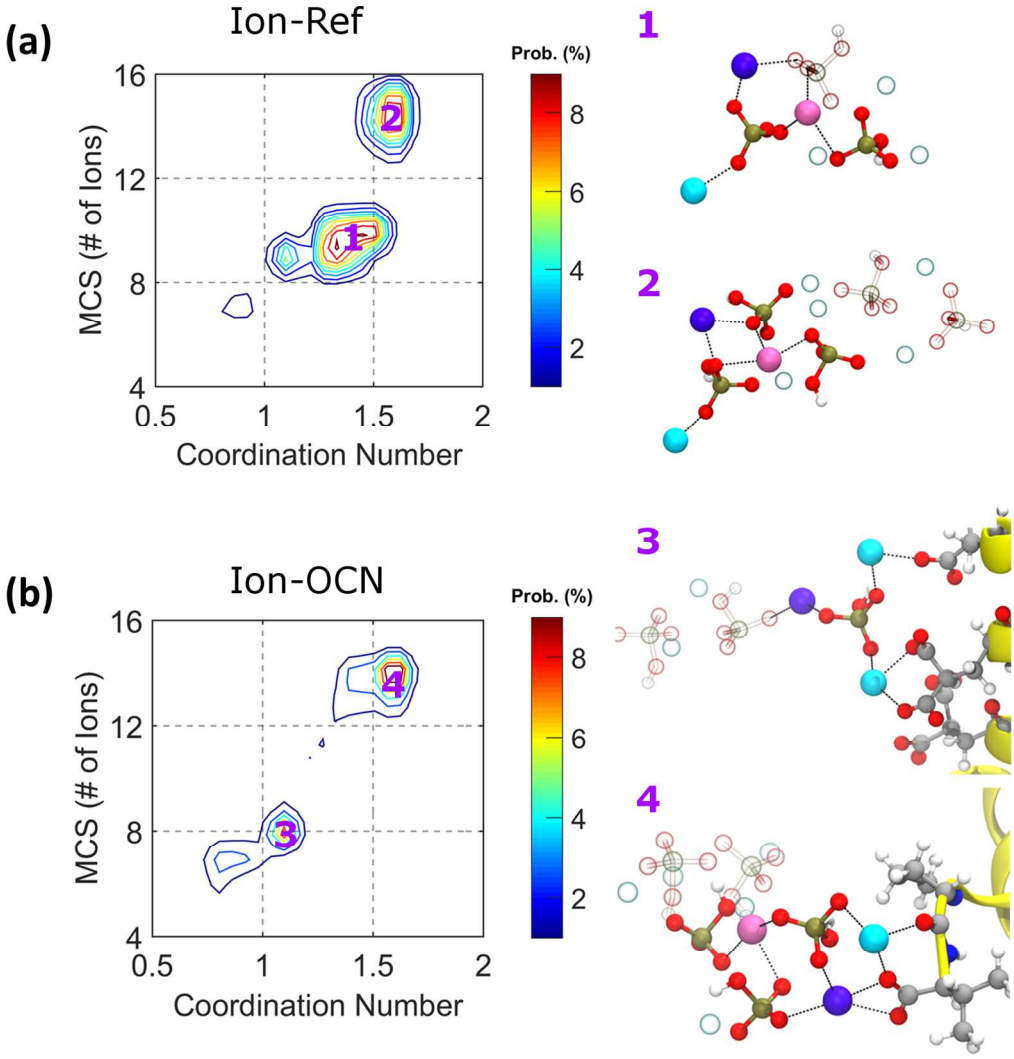


Figure 3. Coordination chemistry and morphology of the ion complexes for (a) Ion-Ref and (b) Ion-OCN simulations. Left: 2-D histograms of the MCS and the coordination number of $HPO_4^{2-}$ to $Ca^{2+}$. The probability distribution of states is indicated by colored contours. Right: the molecular configurations show the representative structures from probability basins. Different coordination environment of $Ca^{2+}$ is highlighted by different colors: cyan: $Ca^{2+}$ coordinated by one $HPO_4^{2-}$; blue: $Ca^{2+}$ coordinated by two $HPO_4^{2-}$; pink: $Ca^{2+}$ coordinated by three $HPO_4^{2-}$. The black dashed lines indicate the potential interatomic bonds between $Ca^{2+}$ and oxygens. For clarity, only one characteristic $Ca^{2+}$ is shown for each coordination environment and the rest are defocused, and water molecules are not shown.

*Comparison of Nucleation Energy Landscape in CaP and CaC Systems*

We have shown above that the monotonic decrease of free energy of ion complex nucleation is true regardless of whether OCN is present. The lack of a free energy barrier for ion complex nucleation is in agreement with previous computational work on the inorganic calcium carbonate (CaC) system[45] where no local free energy minima were identified as the complex grew up to 45 ions.[45] The relative free energy decrease of CaP complex growth from 3 to 13 ions determined here is about 20 $k_bT$, compared to ~ 100 $k_bT$ for the CaC system. This difference may be a result of the different intermolecular force field parameters between $Ca^{2+}/HPO_4^{2-}$ and $Ca^{2+}/CO_3^{2-}$ systems. We note that absolute values of free energies describing atomic level interaction potentials can only be obtained by density functional theory calculations, while in these MD-based simulations, the free energy landscapes obtained are specific to certain molecular geometrical CV. Indeed, the CV introduced in the present study represents the largest complex from a distribution of sizes, which distinguishes it from the one used in the previous study where the size of isolated, discrete ion complexes was defined as the CV. Taken together, these results indirectly imply that the barrier to nucleation lies in the transition of liquid-like pre-nucleation clusters to solid amorphous phase particles, although we re-emphasize that this step has not been studied by simulations in either the previous study on CaC nor in the present study.

The MD simulation of CaC pre-nucleation complexes without any biomolecules present has also shown that the complexes are highly hydrated ionic assemblies favoring branch- or chain-like morphologies.[44] This liquid-like nature of initially formed inorganic CaC complexes has also been demonstrated by Wallace et al, based on the similar diffusivity of these complexes compared to water and individual ions in solution.[45] In interesting

accordance, the complexes observed from our simulations of both Ion-Ref and Ion-OCN systems have elongated rather than spherical shape as discussed above. This concurrence suggests that both CaC and CaP initially form nanosized ion complexes with large solvent-accessible surface area. This highly hydrated state of ion complexes may lead to an energy barrier for their transformation to more compact, solid-phase amorphous particles.

*Dynamics of Ion Complex Growth in Canonical Ensemble*

Obtained by the ensemble-biased techniques of MetaD and US, the present results reveal the free energy landscape of IAC growth. However, the time-elapsed of IAC growth cannot be reflected by the enhanced sampling approaches. To understand the natural dynamics associated with IAC growth and to validate the results from the preceding free energy calculation, we performed conventional MD simulation targeting the nucleation stages of IAC formation. The probability distribution of finding a particular size of IACs sampled over successive time intervals of 10 ns is shown in Figure 4 for Ion-Ref (top) and Ion-OCN (tottom) systems. For both nucleating systems, the distribution is dominated by peaks that have IAC size smaller than 10 ions (average size ~1 nm), indicating the slow aggregation kinetics of ions in the conventional MD simulation. The largest IACs formed in the reference system consist of only about 16-17 ions and these appear after 30 ns, whereas IACs larger than 20 ions are formed in the presence of OCN after 40 ns. Furthermore, there is a wider distribution of IAC sizes in the reference system compared to the OCN system. In the latter case, multiple peaks exist between 2 and 10 ions, followed by almost no IACs of intermediate size and then a peak at 20-22 ions. Thus, the presence of OCN favors the growth of IACs by aggregation of intermediate smaller ones.

We fit the number of IACs in the simulation systems as a function of time (Figure 4b). Similar to the result from previous simulation of CaC nucleation, the decay of IAC number is exponential ($y = y_0 * \exp(-t/\tau) + N$). In the presence of OCN, the number of IACs at equilibrium, N, is smaller than that of the reference system (21 *vs.* 24), confirming that OCN promotes the formation of larger sizes of IACs, in that both systems initially have the same ion concentration. This result confirms that OCN favors IAC growth by aggregation of smaller ones.

Compared to the data from enhanced sampling, the results of conventional MD here reflect the actual physical timescale, mapping to the possible size distribution of IACs that form within nanoseconds, though not necessarily including all the intermediate states. The larger-sized IACs form in the Ion-OCN system (20 to 22 ions, Figure 4a) are a result of the assembly of several smaller IACs that have been captured by MetaD and US simulations (Figure 1 and 2). Combining the observation from conventional MD with the PMF calculated on sufficiently sampled intermediate states, we infer that OCN promotes the enlargement of smaller IACs, which then increases the average size of larger IAC assemblies through particle attachment process, in contrast to the reference system.

In summary, the initial IAC formation in the presence of OCN is thermodynamically favored by binding to OCN's charged side chains, and the subsequent growth of the IACs to larger cluster assemblies is kinetically controlled.

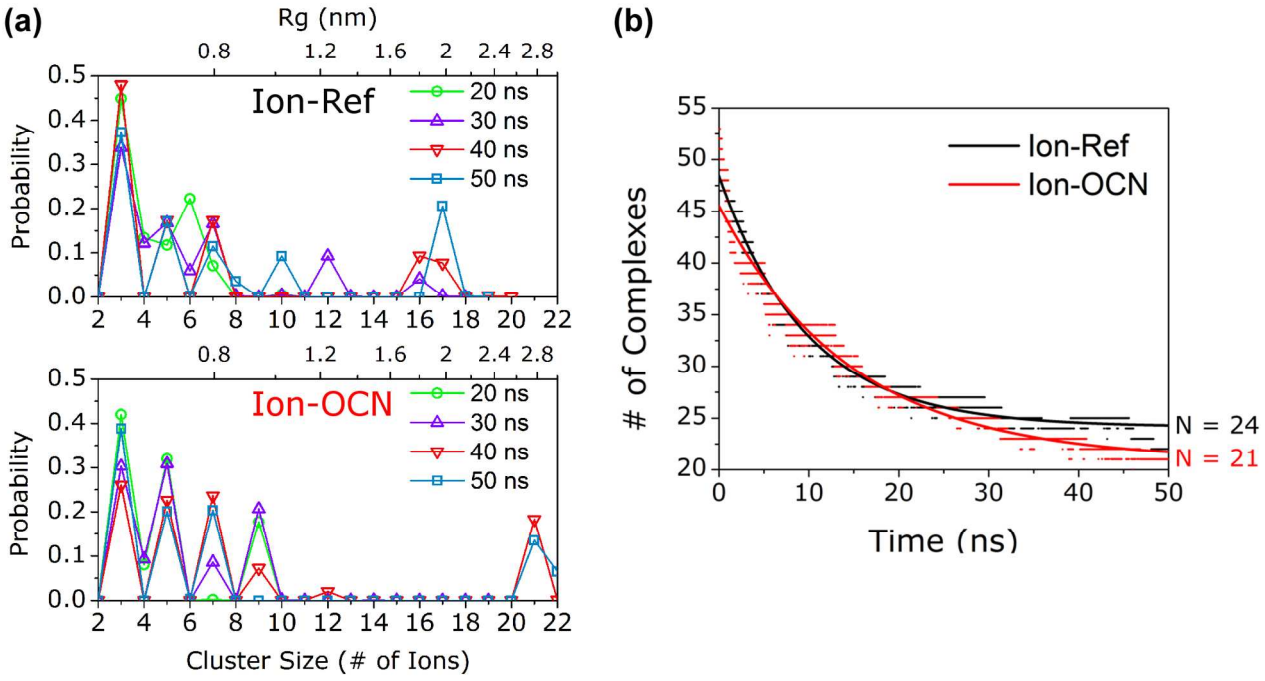


Figure 4. Conventional MD simulations results. (a) Size distributions of CaP IACs sampled over successive time intervals. The histogram at each interval is calculated by considering 5000 configurations spanning 10 ns time, e.g., the data at 20 ns are analyzed based on simulation frames from 10 to 20 ns. Top x-axis marks averaged radius of gyration (Rg) of the CaP complex sampled by corresponding US window. (b) The number of IACs as a function of simulation time. The solid lines are fitted to exponential decay curves ($y= y_0 \times \exp(-t/\tau)+N$), where $y_0$ is the initial number of complexes, $\tau$ is the decay time constant, and N is the hypothetical equilibrated number of complexes with respect to the 50 ns timeframe.

*Cluster Assemblies to Amorphous Calcium Phosphate*

In order to explore the evolution of the system beyond the time-scales accessible by MD simulations, we conducted experimental Dynamic Light Scattering (DLS) measurement on Ion-Ref and Ion-OCN systems. The time-scale of the DLS experiments detects the later stages involved in the aggregation of IACs to forming cluster assemblies and further cluster assembly aggregation to form ACP.[53,54] In Figure S3a, the number mean particle size corresponding to the dominant peak are collected to calculate the histograms. The size distribution of IACs is comparable to previous DLS data reported for CaP nucleation in simulated body fluid (1 to 100 nm).[54] When OCN is present in the nucleating solution, the population of IACs between 50 and 100 nm is much more prominent compared to the reference system. The time evolution of IAC and cluster assembly sizes is displayed in Figure S3b. After the mixing of $Ca^{2+}$ and $HPO_4^{2-}$ solutions, the effect of OCN in facilitating larger IACs can already be seen. As time progresses, IACs aggregate into cluster assemblies, which then form large ACP particles in both systems. During this process, OCN continues to result in larger size compared to the reference system, indicating the promotor role of OCN for larger cluster assembly and ACP formation at a much longer timescale than can be covered by MD simulations.

*Proposed Roles of OCN in Modulating CaP Nucleation*

The computational and experimental results presented here provide alternative role of OCN in regulating CaP nucleation, which has not been captured in previous work and contributes to reconciling several *in vitro* and *ex vivo* studies demonstrating different activities of OCN in HAP nucleation. A proposed role in the literature for the Gla side chains of OCN involves the promotion of HAP formation by offering "lattice match" to the positions of the $Ca^{2+}$ ions on the HAP surface. This proposal was based on results of *in vitro* atomic force microscopic study of brushite-to-HAP dissolution-precipitation, as well as *ex vivo* structural analysis of bone tissue.[20,52] However, our simulation does not support the lattice matching scenario as indicated by the present result that OCN binds IACs, instead of ions, at various charged sites residues, forms elongated IACs, and regulates their further aggregation to amorphous phase. The results of other *in vitro* and *in vivo* studies have revealed that OCN inhibits CaP nucleation, but is much less potent than the established NCP inhibitor, osteopontin.[55-57] Based on our free energy calculation and conventional MD simulations, the interaction of nanosized IACs with OCN stabilizes their growth in the "liquid phase" relative to the reference system. The stabilized IACs and cluster assemblies sustain the continued growth of hydrated ACP particles rather than dehydrating and phase transforming to crystalline HAP. This explains the mild inhibitory effect of OCN compared to stronger NCP inhibitors of bone mineralization.

The present simulation and DLS results show that OCN regulates ACP formation at various scales. Our advanced simulation results show that OCN thermodynamically promotes liquid-like IAC formation at the nanoscale (Figure 5, Stage I), by binding the IACs at various charged side chains. Specifically, excessive surface energy of the cluster-water interface, can

be compensated by the favorable electrostatic interactions between inorganic clusters and protein side chains, which resemble the electrostatic forces within bulk ACP. Moreover, the release of surface-bound water as a result of inorganic-protein binding contributes to increased conformational entropy, lowering the overall free energy as well. In the next stage of ACP formation, OCN kinetically promotes the aggregation of these IACs to form "polymeric" cluster assemblies (Figure 5, Stage II). These results provide a plausible molecular mechanism regarding how organic substrates, in general, reduce the free energy for ACP or ACC formation through the non-classical nucleation pathway[30,58] which are consistent with previous work on inorganic CaP and CaC systems.[26] The third stage involves aggregation of the sub-micron cluster assemblies to form hydrated ACP particles, which is also promoted in the presence of OCN, as demonstrated by the DLS result. The hydrated ACP particles presumably undergo chemistry alteration including dehydration and deprotonation, eventually transforming into crystalline HAP particles. By stabilizing the hydrated IACs and cluster assemblies in liquid state, OCN may delay the final stage involving transformation from hydrated ACP to HAP. We note that although terminal amidation of an OCN-derived peptide is found to promote ACP-to-HAP crystallization,[59] the effect is likely to be different in the scenario of full-length OCN. In sumaary, OCN promotes formation of the initial phase of liquid-like ionic aggregates and their assembly to large liquid-phase ACP during the ACP and HAP nucleation. When the liquid-phase particle reaches a critical size, OCN becomes a mild inhibitor thus delaying the transformation to solid-phase ACP or HAP crystals by OCN binding to the particle and lowering the surface excess free energy of the particle.

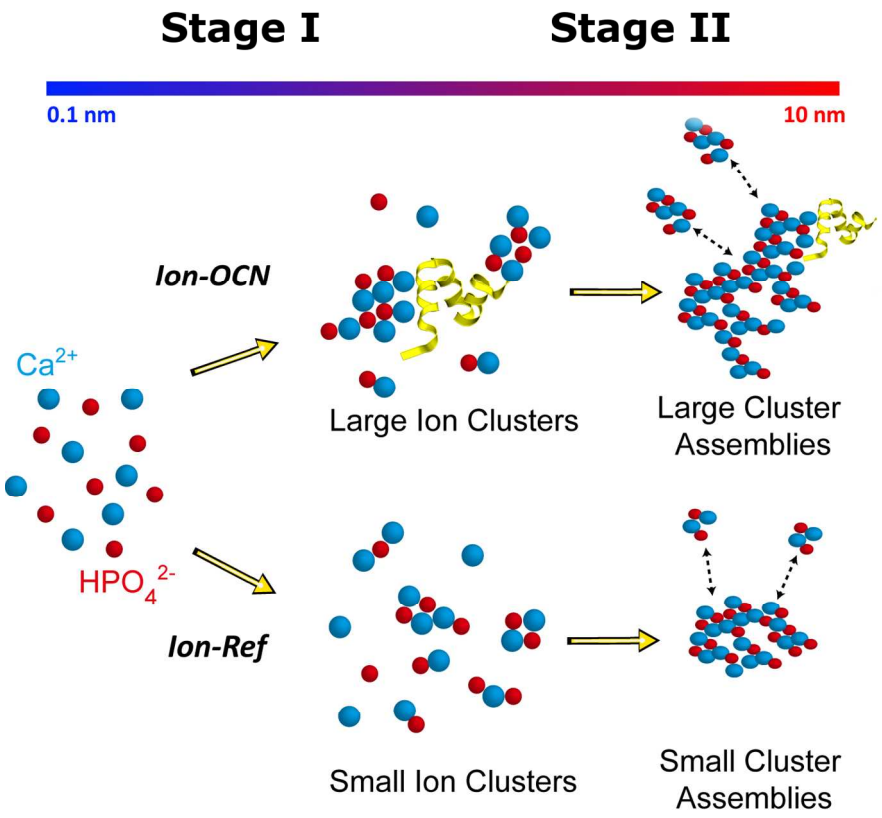


Figure 5. Regulation of early stages of ACP nucleation by OCN. Nucleation sequence progresses from left to right. Stage I: Ions and ion pairs in solution form nanosized IACs which share characteristics with the concept proposed by Habraken et al.[26] The presence of OCN facilitates IAC formation and enlargement. Stage II: IACs aggregate into liquid-like cluster assemblies, dynamically exchange with IACs in the surrounding solution phase (dashed arrows). In the presence of OCN, the exchange species tend to be larger IACs compared to the reference system. In present study, MetaD and US data primarily capture Stage I, and conventional MD and DLS capture Stage I and II.

## 3. Conclusion

Our free energy calculation using advanced MD sampling techniques reveals a promotor effect of OCN on the formation of nanosized CaP IACs under the paradigm of non-classical nucleation theory. The promotion effect is attained by the binding of charged OCN side chains, primarily the N-terminal Gla segment, to ions on the IACs. In addition, the C-terminal Arg residues also exhibit binding potency to the IACs. Such molecular-level interactions lower the excess surface energy of growing IACs and also stabilize their elongated, ribbon-like morphology. Considering the multiple stages involved in HAP nucleation and growth, the activity of OCN in bone formation may depend on its *in vivo* association with the inorganic species and phases present in the mineralizing matrix, besides a previously proposed role as a signaling molecule. Therefore, the effect of OCN expression on bone formation can be rationalized to a certain extent on the basis of OCN-CaP interactions. Our MD simulation and free energy calculation present new microscopic structural and energetic evidence regarding the activity of OCN in HAP crystallization and, more broadly, protein- or peptide-mediated ionic mineral nucleation in general. From a methodology perspective, our practice of combining advanced MD sampling techniques illustrates the potency of computational modeling in approaching the thermodynamics of biomolecule-directed inorganic crystallization and self-assembly.

**Methods**

*Conventional MD.* OCN has 49 amino acids, leading to a molecular weight of ~ 6 kDa. The 3-D crystal structure of human OCN was constructed by taking the high-resolution (2 Å) data of porcine OCN[22] from protein data bank (ID: 1Q8H), and substituting the last two residues at the C-terminal to match the sequence of the human homolog[60] (Figure S1). The protein was placed in the center of a cubic simulation box ($8.9 \times 8.9 \times 8.9$ nm$^3$). Explicit solvation was applied by filling the box with TIP3P water molecules and equilibrated under NPT ensemble for 500 ps. 100 mM $Ca^{2+}$ and $HPO_4^{2-}$ ions were randomly placed in the solvated box by substituting water molecules. $HPO_4^{2-}$ takes ~ 60 % of the phosphate species ($H_2PO_4^-$ takes ~ 40 %) in the extracellular fluid at pH = 7.4. As the formation of ion complexes initiates, $HPO_4^{2-}$ becomes the dominant specie, and therefore $H_2PO_4^-$ was not considered here. To minimize the bias of initial configuration on ion-ion interactions, the relative positions of ions were adjusted to eliminate pairs having $Ca^{2+}$-$HPO_4^{2-}$ distance smaller than 8 Å. 100 mM NaCl ions were also added to the system to mimic the ionic strength of extracellular fluid. The simulations were carried out using GROMACS 4.5.

*Metadynamics.* PLUMED 2.0 program patched to GROMACS 4.5 package was used for MetaD simulation. After another 500 ps NPT equilibration by regular MD, NVT MetaD simulation was conducted for 25 ns using two CVs: 1) the number of $Ca^{2+}$/$HPO_4^{2-}$ ions that were closer than 3 nm to the center of mass of OCN, to enhance the ion-protein binding; 2) the average coordination number of $HPO_4^{2-}$ to $Ca^{2+}$.

We defined a CaP ion cluster of certain size by the following rules: 1) distance between the center of mass of ion-pair 'monomers' is not larger than the average radius of

gyration of ion-pair monomers themselves; 2) every $Ca^{2+}$-$HPO_4^{2-}$ distance within a cluster is smaller than 2.7 Å; and 3) the cluster exists longer than 1 ps.

Different sizes of CaP ion clusters comprised of 3 to 14 ions were observed during the MetaD stage, and were extracted for free energy calculation. Although MetaD greatly enhances the exploration of phase space, possibility remains that certain size or stoichiometry of clusters were more favorably sampled during the simulation. Therefore, we performed three MetaD simulations in parallel, and compared the ion clusters from each simulation to ensure that the extracted structures are representative and equilibrated. In a similar fashion, three separate simulations were also performed for the inorganic reference system (Ion-Ref), in the absence of OCN. The configuration snapshots of different cluster sizes of the OCN system (Ion-OCN) and Ion-Ref system were saved to initiate the following US free energy calculation.

*Umbrella Sampling.* US simulations were carried on PLUMED 2.2[61] in conjunction with GROMACS 4.5[62], which was customized to enable using the Maximum Complex Size (MCS) as the CV for potential of mean force (PMF) calculation. From the aforementioned results of MetaD, 12 configuration snapshots identified as having MCS of 3 to 14 were first equilibrated for 1 ns by restraining the $Ca^{2+}$ and $HPO_4^{2-}$ ions with a harmonic potential constant of 1000 $kJ \cdot mol^{-1} \cdot nm^{-2}$, which is heavy enough to prevent structural rearrangement of clusters. Then, 12 US windows were introduced, starting with corresponding MCS as the target CV. Different umbrella potential constants were tested to target the CV at each designated MCS number while maintaining sufficient CV histogram overlap between windows. A 10 $kJ \cdot mol^{-1}$ value permitted such overlap with good statistical accuracy and was therefore applied to each window. A 4 ns NVT simulation was performed on each window

with CV and restraining force recorded every 20 ps. The recorded data were reweighted by Multi-states Bennett Acceptance Ratio (MBAR) method[50,63]. In brief, the bias introduced by umbrella potential restraint was removed by an iterative algorithm to recover the system potential energy in original canonical ensemble, which was used to generate the unbiased PMF. The unbiased PMF thus indicates the free energy landscape for the spontaneous growth of CaP clusters in solution.

**List of Abbreviations:**

ACC – Amorphous Calcium Carbonate

ACP – Amorphous Calcium Phosphate

CaC – Calcium Carbonate

CaP – Calcium Phosphate

CN – Coordination Number

CV – Collective Variable

DLS – Dynamic Light Scattering

HAP – Hydroxyapatite

IAC – Ion Association Complex/Cluster

MBAR – Multi-state Bennet Acceptance Ratio

MCS – Maximum Cluster Size

MD – Molecular Dynamics

MetaD – Metadynamics

NCP – Non-collagenous Protein

OCN – Osteocalcin

PMF – Potential of Mean Force

US – Umbrella Sampling

**Acknowledgments**

We sincerely thank Prof. Bill Landis for helpful discussions. N.S. acknowledges funding support by NSF DMR Biomat 0906817 and University of Akron Ohio Research Scholar Funding. Z.X. acknowledges funding support by National Natural Science Foundation of China (No. 21606122 and 21771106) and Natural Science Foundation of Jiangsu Province (No. BK20160995). The authors also appreciate the support of Frank Kelley Fellowship to W. Z. and Robert E. Helm Jr. Fellowship to Z. W. and X. Z. Computational resources were generously provided by Ohio Supercomputer Center (Grant PBS0286, PAA0012).

**Conflicts of interest**

The authors declare no conflict of interest.

## References


(1) Thacker, V. V.; Herrmann, L. O.; Sigle, D. O.; Zhang, T.; Liedl, T.; Baumberg, J. J.; Keyser, U. F. *Nature Communications* **2014**, *5*.

(2) Nair, A. K.; Gautieri, A.; Chang, S.-W.; Buehler, M. J. *Nature Communications* **2013**, *4*, 1724.

(3) Pinheiro, A. V.; Han, D.; Shih, W. M.; Yan, H. *Nat Nano* **2011**, *6*, 763.

(4) Fratzl, P. *Nature Materials* **2008**, *7*, 610.

(5) Weiner, S.; Dove, P. M. *Reviews in Mineralogy & Geochemistry* **2003**, *54*, 1.

(6) George, A.; Veis, A. *Chemical Reviews* **2008**, *108*, 4670.

(7) Addadi, L.; Weiner, S. *Nature* **2001**, *411*, 753.

(8) Boskey, A. L. *Connective Tissue Research* **2003**, *44*, 5.

(9) Michenfelder, M.; Fu, G.; Lawrence, C.; Weaver, J. C.; Wustman, B. A.; Taranto, L.; Evans, J. S.; Morse, D. E. *Biopolymers* **2003**, *70*, 522.

(10) Silver, F. H.; Landis, W. J. *Connective Tissue Research* **2011**, *52*, 242.

(11) Beniash, E. *Wiley Interdisciplinary Reviews: Nanomedicine and Nanobiotechnology* **2011**, *3*, 47.

(12) Nudelman, F.; Pieterse, K.; George, A.; Bomans, P. H. H.; Friedrich, H.; Brylka, L. J.; Hilbers, P. A. J.; de With, G.; Sommerdijk, N. A. J. M. *Nature Materials* **2010**, *9*, 1004.

(13) Xu, Z.; Yang, Y.; Wang, Z.; Mkhonto, D.; Shang, C.; Liu, Z.-P.; Cui, Q.; Sahai, N. *Journal of Computational Chemistry* **2014**, *35*, 70.

(14) Jaeger, C.; Groom, N. S.; Bowe, E. A.; Horner, A.; Davies, M. E.; Murray, R. C.; Duer, M. J. *Chemistry of Materials* **2005**, *17*, 3059.

(15) Yu, X.; Khalil, A.; Dang, P. N.; Alsberg, E.; Murphy, W. L. *Advanced Functional Materials* **2014**, *24*, 3082.

(16) Heywood, B. R.; Sparks, N. H.; Shellis, R. P.; Weiner, S.; Mann, S. *Connect Tissue Res.* **1990**, *25*, 103.

(17) Hess, B.; Kutzner, C.; van der Spoel, D.; Lindahl, E. *J. Chem. Theor. Comput.* **2008**, *4*, 435.

(18) Zurick, K. M.; Qin, C.; Bernards, M. T. *Journal of Biomedical Materials Research Part A* **2013**, *101A*, 1571.

(19) Wang, Z.; Xu, Z.; Zhao, W.; Sahai, N. *Journal of Materials Chemistry B* **2015**, *3*, 9157.

(20) Hauschka, P. V.; Lian, J. B.; Cole, D. E.; Gundberg, C. M. *Physiological Reviews* **1989**, *69*, 990.

(21) Neve, A.; Corrado, A.; Cantatore, F. P. *Journal of Cellular Physiology* **2013**, *228*, 1149.

(22) Hoang, Q. Q.; Sicheri, F.; Howard, A. J.; Yang, D. S. C. *Nature* **2003**, *425*, 977.

(23) Ducy, P.; Desbois, C.; Boyce, B.; Pinero, G.; Story, B.; Dunstan, C.; Smith, E.; Bonadio, J.; Goldstein, S.; Gundberg, C.; Bradley, A.; Karsenty, G. *Nature* **1996**, *382*, 448.

(24) Murshed, M.; Schinke, T.; McKee, M. D.; Karsenty, G. *The Journal of Cell Biology* **2004**, *165*, 625.

(25) Chen, L.; Jacquet, R.; Lowder, E.; Landis, W. J. *Bone*, *71*, 7.

(26) Habraken, W. J. E. M.; Tao, J.; Brylka, L. J.; Friedrich, H.; Bertinetti, L.; Schenk, A. S.; Verch, A.; Dmitrovic, V.; Bomans, P. H. H.; Frederik, P. M.; Laven, J.; van der Schoot,

P.; Aichmayer, B.; de With, G.; DeYoreo, J. J.; Sommerdijk, N. A. J. M. *Nature Communications* **2013**, *4*, 1507.

(27) Dey, A.; Bomans, P. H. H.; Müller, F. A.; Will, J.; Frederik, P. M.; de With, G.; Sommerdijk, N. A. J. M. *Nature Materials* **2010**, *9*, 1010.

(28) Gebauer, D.; Cölfen, H. *Nano Today* **2011**, *6*, 564.

(29) De Yoreo, J. J.; Gilbert, P. U. P. A.; Sommerdijk, N. A. J. M.; Penn, R. L.; Whitelam, S.; Joester, D.; Zhang, H.; Rimer, J. D.; Navrotsky, A.; Banfield, J. F.; Wallace, A. F.; Michel, F. M.; Meldrum, F. C.; Cölfen, H.; Dove, P. M. *Science* **2015**, *349*.

(30) Wang, L.; Nancollas, G. H. *Chemical Reviews* **2008**, *108*, 4628.

(31) Jiang, S.; Pan, H.; Chen, Y.; Xu, X.; Tang, R. *Faraday discussions* **2015**, *179*, 451.

(32) Gebauer, D.; Kellermeier, M.; Gale, J. D.; Bergstrom, L.; Colfen, H. *Chemical Society reviews* **2014**, *43*, 2348.

(33) Davey, R. J.; Schroeder, S. L. M.; ter Horst, J. H. *Angewandte Chemie International Edition* **2013**, *52*, 2166.

(34) Sadeghi, O.; Zakharov, L. N.; Nyman, M. *Science* **2015**, *347*, 1359.

(35) Ruther, R. E.; Baker, B. M.; Son, J.-H.; Casey, W. H.; Nyman, M. *Inorganic Chemistry* **2014**, *53*, 4234.

(36) Nudelman, F.; Pieterse, K.; George, A.; Bomans, P. H. H.; Friedrich, H.; Brylka, L. J.; Hilbers, P. A. J.; de With, G.; Sommerdijk, N. A. J. M. *Nat Mater* **2010**, *9*, 1004.

(37) Xu, Z.; Yang, Y.; Zhao, W.; Wang, Z.; Landis, W. J.; Cui, Q.; Sahai, N. *Biomaterials* **2015**, *39*, 59.

(38) Yang, Y.; Cui, Q.; Sahai, N. *Langmuir* **2010**, *26*, 9848.

(39) Zhao, W.; Xu, Z.; Cui, Q.; Sahai, N. *Langmuir* **2016**.

(40) Zhao, W.; Xu, Z.; Sahai, N. In *Molecular Modeling of Geochemical Reactions: An Introduction*; Kubicki, J., Ed.; Wiley: 2016, p 311.

(41) Yang, Y.; Xu, Z.; Cui, Q.; Sahai, N. In *Biomineralization Sourcebook*; DiMasi, E., Gower, L. B., Eds.; CRC Press: 2014, p 265.

(42) Mendez-Villuendas, E.; Bowles, R. K. *Physical Review Letters* **2007**, *98*, 185503.

(43) Radhakrishnan, R.; Trout, B. L. *Journal of the American Chemical Society* **2003**, *125*, 7743.

(44) Demichelis, R.; Raiteri, P.; Gale, J. D.; Quigley, D.; Gebauer, D. *Nature Communications* **2011**, *2*, 590.

(45) Wallace, A. F.; Hedges, L. O.; Fernandez-Martinez, A.; Raiteri, P.; Gale, J. D.; Waychunas, G. A.; Whitelam, S.; Banfield, J. F.; De Yoreo, J. J. *Science* **2013**, *341*, 885.

(46) Barducci, A.; Bonomi, M.; Parrinello, M. *Wiley Interdisciplinary Reviews: Computational Molecular Science* **2011**, *1*, 826.

(47) Quigley, D.; Freeman, C. L.; Harding, J. H.; Rodger, P. M. *Journal of Chemical Physics* **2011**, *134*, 044703.

(48) Martonak, R.; Donadio, D.; Oganov, A. R.; Parrinello, M. *Nat Mater* **2006**, *5*, 623.

(49) Sleutel, M.; Van Driessche, A. E. S. *Proceedings of the National Academy of Sciences of the United States of America* **2014**, *111*, 546.

(50) Fajer, M.; Swift, R.; McCammon, J. A. *Journal of Computational Chemistry* **2009**, *30*, 1719.

(51) Michel, J.; Tirado-Rives, J.; Jorgensen, W. L. *Journal of the American Chemical Society* **2009**, *131*, 15403.

(52) Flade, K.; Lau, C.; Mertig, M.; Pompe, W. *Chemistry of Materials* **2001**, *13*, 3596.

(53) de Bruyn, J. R.; Goiko, M.; Mozaffari, M.; Bator, D.; Dauphinee, R. L.; Liao, Y.; Flemming, R. L.; Bramble, M. S.; Hunter, G. K.; Goldberg, H. A. *PLoS ONE* **2013**, *8*, e56764.

(54) Oyane, A.; Onuma, K.; Ito, A.; Kim, H. M.; Kokubo, T.; Nakamura, T. *Journal of biomedical materials research. Part A* **2003**, *64*, 339.

(55) Hunter, G. K.; Hauschka, P. V.; Poole, A. R.; Rosenberg, L. C.; Goldberg, H. A. *Biochemical Journal* **1996**, *317*, 59.

(56) Boskey, A. L.; Gadaleta, S.; Gundberg, C.; Doty, S. B.; Ducy, P.; Karsenty, G. *Bone*, *23*, 187.

(57) Murshed, M.; Schinke, T.; McKee, M. D.; Karsenty, G. *J Cell Biol* **2004**, *165*, 625.

(58) Hu, Q.; Nielsen, M. H.; Freeman, C. L.; Hamm, L. M.; Tao, J.; Lee, J. R. I.; Han, T. Y. J.; Becker, U.; Harding, J. H.; Dove, P. M.; De Yoreo, J. J. *Faraday discussions* **2012**, *159*, 509.

(59) Hosseini, S.; Naderi-Manesh, H.; Mountassif, D.; Cerruti, M.; Vali, H.; Faghihi, S. *Journal of Biological Chemistry* **2013**, *288*, 7885.

(60) Nielsen-Marsh, C. M.; Richards, M. P.; Hauschka, P. V.; Thomas-Oates, J. E.; Trinkaus, E.; Pettitt, P. B.; Karavanić, I.; Poinar, H.; Collins, M. J. *Proceedings of the National Academy of Sciences of the United States of America* **2005**, *102*, 4409.

(61) Tribello, G. A.; Bonomi, M.; Branduardi, D.; Camilloni, C.; Bussi, G. *Computer Physics Communications* **2014**, *185*, 604.

(62) Pronk, S.; Pall, S.; Schulz, R.; Larsson, P.; Bjelkmar, P.; Apostolov, R.; Shirts, M. R.; Smith, J. C.; Kasson, P. M.; van der Spoel, D.; Hess, B.; Lindahl, E. *Bioinformatics (Oxford, England)* **2013**, *29*, 845.

(63) Tan, Z.; Gallicchio, E.; Lapelosa, M.; Levy, R. M. *The Journal of Chemical Physics* **2012**, *136*, 144102.